Available online at www.sciencedirect.com
SCIENCE DIRECT®
International Journal of Heat and Fluid Flow 24 (2003) 698–708
International Journal of HEAT AND FLUID FLOW
www.elsevier.com/locate/ijhff

Unsteady loss in a high pressure turbine stage

S.J. Payne [a,*], R.W. Ainsworth [a], R.J. Miller [b,1], R.W. Moss [c,1], N.W. Harvey [d]

[a] Department of Engineering Science, University of Oxford, Oxford OX1 3PJ, UK
[b] Whittle Laboratory, University of Cambridge, Cambridge, UK
[c] Department of Marine Science and Technology, University of Newcastle upon Tyne, UK
[d] Rolls-Royce plc., Derby, UK

Received 6 November 2002; accepted 14 March 2003

Abstract

An investigation into the unsteady losses in a high pressure turbine stage has been performed experimentally at engine-representative conditions. This has been done by making time-resolved measurements of entropy at stage exit at all vane and rotor-relative positions over a wide range of radial height. Due to the considerable difficulty of obtaining accurate measurements at engine-representative conditions, these measurements provide a unique set of experimental data. Five distinct flow features have been identified and their effects on the stage efficiency estimated, showing good overall agreement with an independent efficiency measurement. Comparisons with a particular numerical prediction of the flow field, Unstrest, have shown very good agreement in both the flow structure and the entropy generation. Only the rotor dependence of the loss mechanisms is examined here: the vane dependence will be presented in a subsequent paper.

Keywords: Unsteady flow; Loss mechanisms; Entropy measurements; Efficiency

1. Introduction

The flow field in the high pressure turbine stage is very complex, due to the high degree of unsteadiness and the effects of blade row interaction, and is thus still far from being understood thoroughly. There is still much experimental work to be performed on understanding the formation of loss, particularly with regard to the effects of blade row interaction. Although numerical predictions have been proved to be valuable in understanding the flow structure, it is important to gauge their accuracy in an absolute sense by comparison with experimental measurements, both for individual loss features and the stage efficiency. It is thus vital that further experimental measurements are made at engine-representative conditions, to understand and to quantify the losses and to validate numerical predictions. This is the aim of this work presented here.

Following the definition by Denton (1993), any flow feature that reduces the stage efficiency will be termed loss. Since the efficiency is usually defined as the ratio of the actual work output to the isentropic work output, only rises in entropy can reduce the efficiency. As rises in entropy are only caused by heat transfer or flow irreversibility, "the only rational measure of loss in an adiabatic machine is entropy creation" (Denton, 1993). The measurement of entropy should thus be a primary goal of loss mechanism research.

The advantages of using entropy to investigate loss are that it is independent of the frame of measurement and that it can be converted to efficiency if only one other property of state is known:

$$\eta = \frac{1 - \left(p_{\mathrm{r}} \mathrm{e}^{(s_2 - s_1)/R}\right)^{(\gamma-1)/\gamma}}{1 - \left(p_{\mathrm{r}}\right)^{(\gamma-1)/\gamma}}. \tag{1}$$

The disadvantages are that it cannot be measured directly and that only changes in entropy have any meaning, necessitating the measurement of four flow parameters:

* Corresponding author. Tel.: +44-1865-27-3095; fax: +44-1865-27-3905.
E-mail address: stephen.payne@univ.ox.ac.uk (S.J. Payne).
[1] Formerly at the Department of Engineering Science, University of Oxford.

0142-727X/$ - see front matter © 2003 Elsevier Inc. All rights reserved.
doi:10.1016/S0142-727X(03)00027-4

Nomenclature

h	heat transfer coefficient
l	length
m	mass
n	constant
p	pressure
r	radius
s	specific entropy
u	velocity
x	length
A	area; constant
B	constant
C	constant
D	constant
E	voltage
M	Mach number
N	rotational speed
Nu	Nusselt number
Q	heat transfer
R	gas constant
Re	Reynolds number
S	entropy
T	temperature
γ	ratio of specific heats
η	efficiency; recovery factor
θ	angle
ρ	density

Subscripts

m	mean
o	total conditions
r	ratio
w	wall; wire
BS	blade surface
P	pitch
1	HP vane inlet conditions
2	HP vane exit conditions
3	HP rotor exit conditions

Superscripts

$\bullet$	time differential
$-$	mean
$*$	choked
$'$	change

$$\frac{s_2 - s_1}{R} = \left(\frac{\gamma}{\gamma - 1}\right) \ln\left(\frac{T_{o2}}{T_{o1}}\right) - \ln\left(\frac{p_{o2}}{p_{o1}}\right). \quad (2)$$

We assume that air is an ideal gas throughout this paper.

There are three fluid dynamic processes that create entropy, and hence loss: viscous friction, heat transfer and non-equilibrium processes (Denton, 1993). To provide a clearer physical insight into the flow field, however, loss is more conveniently divided into its various components, each of which is outlined briefly:

Two-dimensional loss:

1. Boundary layer loss: Entropy is generated by shear stresses in the boundary layer, depending upon the state of the boundary layer. Estimates of the loss have been made by Wallace and Davies (1997) and Moore and Gregory-Smith (1996) amongst others.
2. Shock loss: Entropy is generated by shock waves in the flow field at high Mach numbers. This is normally the smallest loss component.
3. Mixing loss: Entropy is generated by mixing of the flow field behind the blade trailing edge. Estimates of the loss have been made by Roberts and Denton (1996) and Prato and Lakshminarayana (1992) amongst others.

The breakdown and dependence on Mach number of the loss components in a two-dimensional cascade with a similar blade profile to that used here have been examined by Mee et al. (1990).

Three-dimensional loss:

1. End wall loss: Entropy is generated by the end wall boundary layers and the secondary flow structure. The loss is highly dependent upon the secondary flow field, which has been examined in considerable detail by Sieverding (1984), Sharma and Butler (1986) and Yamamoto et al. (1995) amongst others.
2. Tip leakage loss: Entropy is generated by the tip leakage flow through unshrouded rotor tip gaps. This loss is highly dependent upon the size of the tip gap and strongly influences the other end wall loss. The loss has been examined by Bindon (1988) and Yaras and Sjolander (1991) amongst others.

However, despite our often relatively good understanding of the flow field, the accuracy of loss predictions is still low, as the entropy generation cannot be estimated accurately. Although numerical predictions are valuable in predicting the flow structure, there are difficulties in predicting the loss accurately, due to errors in predicting the boundary layers, transition and the base pressure coefficient, as well as due to false entropy generation due to numerical dissipation. There are also very few experimental measurements of unsteady loss at engine-representative conditions with which to validate either loss correlations or numerical predictions.

Under engine-representative conditions, blade row interaction effects are also important, since the mixing of the flow is affected and the rotation of alternate blade rows introduces unsteadiness: although these do not necessarily cause loss, they are likely to affect the loss behaviour significantly (Hodson, 1984). The main interaction effects are wake interaction, shock wave interaction, potential flow interaction and secondary flow interaction. However, since little experimental work has been performed, the level of understanding of interaction is far behind that of the losses found in isolated blade rows (Denton, 1993). There is thus still much work to be performed on investigating unsteady loss mechanisms and the effects of blade row interaction under engine-representative conditions. This is the aim of the experimental results presented here.

2. Experimental facility

In order to make relevant and accurate unsteady loss measurements, the necessary flow conditions must be modelled correctly. The facility used here is the Oxford Rotor Facility, which was designed to simulate engine-representative conditions by matching the required non-dimensional conditions for a very short period of time (Ainsworth et al., 1988). The working section comprises a 0.62 scale version of the Rolls-Royce RT27a blade profile for the High Pressure (HP) turbine stage and the first blade row from a typical Intermediate Pressure (IP) stage, Fig. 1. Since the rotor is unbraked and thus continuously accelerating, the facility is at the required flow conditions for only approximately 15 ms.

Dimensional analysis shows that there are only four dependent parameters that must be matched to simulate

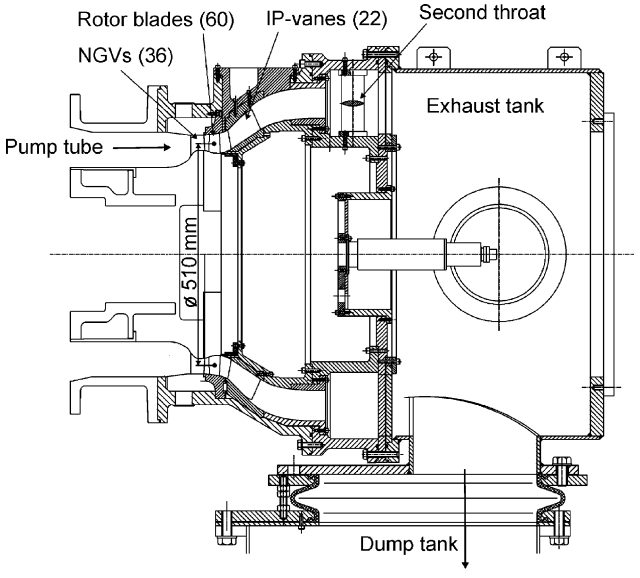

Fig. 1. Oxford Rotor Facility working section.

Table 1
Pseudo-non-dimensional operating point parameters

Specific speed	Pressure ratio	Reynolds number	Temperature ratio
$\frac{N}{\sqrt{T_{o1}}}$	$\frac{p_{o1}}{p_3}$	Re_2	$\frac{T_{o1}}{T_w}$
460.49 rpm/$\sqrt{K}$	3.12	2.7×10^6	1.3

the required engine-representative conditions (Sheard, 1989). Removal of the parameters that remain unchanged from each run gives the necessary pseudo-non-dimensional operating point parameters, Table 1. The Nozzle Guide Vane exit Reynolds number is based on absolute conditions and the axial chord.

In parallel with the experimental measurements, considerable work has been performed on numerical predictions of the flow field. When taken together, they provide a development cycle: the predicted flow structure can be used to aid the interpretation of the experimental results, which in turn evaluate the accuracy of the predictions. This is of crucial importance for the loss, since the code must be able to predict loss accurately if improvements in efficiency are to be assessed numerically.

The code used here, Unstrest, is three-dimensional, viscous and unsteady. It solves a thin shear layer model of the Navier–Stokes equations with the viscous terms evaluated every time step and turned into body force terms for momentum and source terms for energy. The structured grid is formed by the rotation of points defined in two dimensions about the turbine axis: meridional, i.e. pseudo-streamwise, and pseudo-radial. The code uses a 'time-marching' solution scheme in which one blade row gradually rotates relative to the other with flow parameters being interpolated across a sliding plane between the two grids (Denton, 1990). The version of Unstrest used here was developed by Denton but includes some modifications made at Rolls-Royce plc.

The prediction used here, termed Grid 78, has been run at the correct operating conditions with the correct vane–rotor blade ratio of 3:5 and contains approximately 1.6 million nodes. The 2.25% tip gap/span is also modelled: this is important for assessing the impact of the tip leakage flow on the stage efficiency. Since the focus here is on the loss mechanisms within the HP stage, the downstream vane and swan-necked duct have been omitted from these predictions.

3. Instrumentation

Since entropy cannot be measured directly, two properties of state are required: normally total pressure and total temperature, Eq. (2). Although the measurement of total pressure at a high bandwidth is a well-established technique, it has proved to be considerably

harder to measure total temperature at a similar bandwidth. The aspirating probe was thus originally designed to measure unsteady total temperature at high frequencies (Ng and Epstein, 1983). Although thin film heat transfer gauges (Buttsworth et al., 1997) are now an alternative method of measuring total temperature at high frequencies, the aspirating probe remains the only means of simultaneously measuring total pressure and total temperature both spatially and temporally. This is crucial in obtaining the necessary measurement accuracy, as shown later. The other advantages associated with the aspirating probe include a high frequency response, good spatial resolution, small sensitivity to flow angle and a reduction in the effects of probe blockage.

The aspirating probe essentially consists of two hot wires placed upstream of an orifice, Fig. 2. By maintaining a low pressure downstream of the orifice, it is choked and the probe 'sucks' in the flow passing towards it. By calculating the mass flow for a given total pressure, total temperature and Mach number, the mass flow at the choked orifice and the hot wire plane can be equated to give

$$(\rho u)_{\mathrm{w}} = \sqrt{\frac{\gamma}{R}}\frac{p_{\mathrm{o}}}{\sqrt{T_{\mathrm{o}}}}\frac{A^*}{A_{\mathrm{w}}}\left(\frac{2}{\gamma+1}\right)^{(\gamma+1)/[2(\gamma-1)]}. \tag{3}$$

The Reynolds number at the hot wire plane is thus dependent solely upon the total pressure and total temperature. The Mach number is fixed by the area ratio:

$$M_{\mathrm{w}}\left(1+\frac{\gamma-1}{2}M_{\mathrm{w}}^2\right)^{-(\gamma+1)/[2(\gamma-1)]} = \frac{A^*}{A_{\mathrm{w}}}\left(\frac{\gamma+1}{2}\right)^{-(\gamma+1)/[2(\gamma-1)]}. \tag{4}$$

For a hot wire in a constant Mach number flow, the Nusselt number, and hence the hot wire voltage, is solely dependent upon the Reynolds number, when used with Constant Temperature Anemometry, see for example Bruun (1995). When placed inside the aspirating probe, hot wires can thus be used to measure the Reynolds number, using the general relationship between Nusselt number and Reynolds number for a given Mach number (Collis and Williams, 1959):

$$Nu = A + BRe^n. \tag{5}$$

When combined with the standard hot wire equation, this gives the aspirating probe calibration equation:

$$E^2 = \left[C\left(\frac{p_{\mathrm{o}}}{\sqrt{T_{\mathrm{o}}}}\right)^n + D\right](T_{\mathrm{m}} - \eta T_{\mathrm{o}}), \tag{6}$$

where the recovery factor, η, is the ratio of recovery temperature to total temperature and C, D and n are constants. These constants are all found by calibration, despite η being a known function of Mach number, to give the greatest accuracy. Two hot wires are thus required to measure both total pressure and total temperature. Although the wire temperatures should be far apart to give a high level of measurement accuracy, there is a lower limit due to the need for a high bandwidth and an upper limit due to the melting temperature of the wire.

The basic design of the aspirating probe used here follows that of Ng and Epstein (1983) with the probe being made as small as possible to fit between closely coupled blade rows. Platinum-plated tungsten wire of diameter 5 μm was used, since this is less prone to drift and has a high yield strength and temperature coefficient of resistance: all of which improve the measurement accuracy. The wire length to diameter ratio was 240, to reduce conduction effects whilst keeping a high spatial resolution. The wires were placed perpendicular to the rotor trailing edge and were less than 0.5 mm apart. The Mach number at the hot wire plane was set at the mean rotor exit value of 0.45 to reduce blockage effects. The probe head was made of Perspex, giving as smooth as possible both internal and external probe surfaces, thus preventing any spurious local entropy generation and improving the angle sensitivity. Although we have not tested the aspirating probe for the effects of variations in flow angle, the findings of Ng and Epstein (1983) that there is negligible change in probe behaviour as the flow angle is varied within ±20° at the correct freestream Mach number indicate that this effect is small outside the tip region.

The wire temperatures were set at approximately 350 and 550 K to give the greatest measurement accuracy, the mean total temperature at the measurement plane being approximately 295 K. To remove noise and to ensure that the bandwidths of the two hot wires were equal, all the data was filtered using a 100 FIR low-pass filter with a cut-off frequency of 40 kHz: approximately the bandwidth of the lower temperature hot wire.

The probe is calibrated using a dedicated chamber designed and built by Brayton (1996), which allows wide

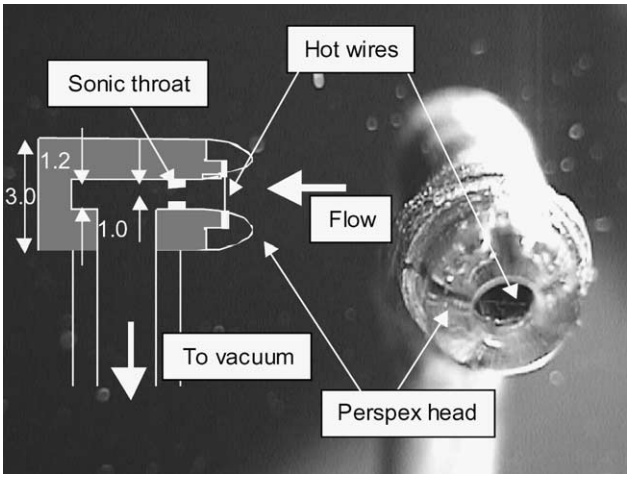

Fig. 2. Oxford aspirating probe design, dimensions in mm.

ranges of total pressure and total temperature to be set independently. By taking a set of data points in the range 2–4 bar and 20–40 °C, a least-squares-error approach is used to provide a fit to the calibration equation. A detailed analysis of all the possible sources of error has shown that the RMS errors in total pressure and total temperature are approximately 0.80% and 0.14% respectively: since the Mach number is constant, these are also the RMS errors in pressure and temperature. These errors correspond to standard deviations in entropy/R and stage efficiency of 0.013 and 1.2%, for a stage total pressure ratio of 2.5 (Payne, 2001). Since errors in total pressure and total temperature magnify noticeably when transformed into efficiency, great care has to be taken to ensure that entropy measurements are sufficiently accurate to resolve loss features.

However, there is a significant high frequency effect in hot wire anemometry, due to the attenuation of heat transfer by conduction from the hot wire to the probe supports (Parantheon et al., 1983). A theoretical examination of this effect has led to the derivation of a compensation factor, which must be used when measuring flow phenomena above a frequency of approximately 1 Hz. When the hot wires are placed inside the aspirating probe, there is a second high frequency effect, due to the fluctuations in the flow field inside the probe being constrained by a constant throat Mach number. This effect cannot be predicted easily and has thus been measured experimentally, leading to an aspirating probe transfer function that must be inverted when processing the measurements made with the aspirating probe. This is outlined in more detail in Payne (2001).

The aspirating probe has previously been used to measure entropy by relatively few authors, primarily in compressors running at lower speeds than those used in the Oxford Rotor Facility. These include Ng and Epstein (1984) and Alday et al. (1993), where the wake region was shown by a rise in entropy, although an extra semiconductor probe was required to give more accurate results. This extra probe was shown by Van Zante et al. (1994) to be unnecessary if care was taken in the design and calibration of the aspirating probe. Van Zante et al. (1994) also presented stationary measurements of total pressure and total temperature, but did not present entropy: likewise Suryavamshi et al. (1996), although they calculated the local isentropic efficiency. Similarly Brouckaert (1998) used the aspirating probe in the facility at VKI behind a turbine stage at higher rotational speeds without attempting to present entropy traces. Thin film heat transfer gauges were used in conjunction with a semiconductor pressure probe by Buttsworth et al. (1997) but again only to present total pressure and total temperature. There have as yet been no accurate entropy traces at the high frequencies found in turbomachines. The experimental measurements presented herein thus provide a unique set of data.

4. Mid-height flow field

Before examining the aspirating probe measurements, it is valuable to look at previous high frequency experimental measurements taken with the same blade rows at the same operating conditions. The Schlieren photograph of the flow field behind a stationary cascade of blades with the same mid-height profile as the rotor blades, Fig. 3, shows that there are two major flow phenomena at approximately 0% and 40% rotor phase: the shock wave and the wake (Miller et al., 2003). The shock wave, which occurs in the rotor relative frame, is shown by rises in total pressure and total temperature in the absolute frame. These are due to the pressure difference between the suction and pressure surfaces in the relative frame and are largely isentropic since the shock wave is very weak, whereas the wake is expected to cause a large rise in entropy.

The ensemble averaged flow fluctuations in measured total pressure, total temperature and the absolute entropy/R at mid-height obtained using the aspirating probe are shown in Fig. 4. The total temperature fluctuations are scaled by a factor of 3.5, to give entropy/R as the difference between the plots of scaled total temperature and total pressure. The signals were ensemble averaged to give the greatest accuracy and plotted over three rotor blades for clarity. This clearly shows the two effects seen in Fig. 3: the shock wave with large rises in total pressure and total temperature, and the wake, with a large rise in entropy. The advantage of simultaneously measuring total pressure and total temperature in the aspirating probe is shown by the small size of entropy fluctuations in comparison with the total pressure and total temperature fluctuations: any measurement error in the phase between total pressure and total temperature will thus be enormously magnified in the error in entropy. This will almost inevitably occur unless the

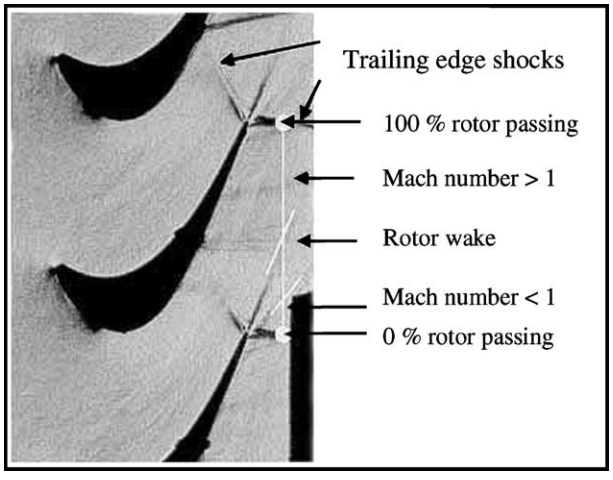

Fig. 3. Schlieren photograph of flow structure at mid-height.

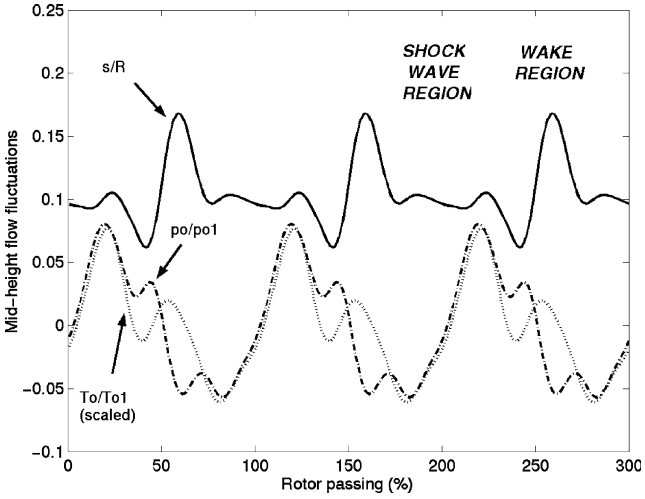

Fig. 4. Aspirating probe measurements of total pressure, total temperature and entropy/R.

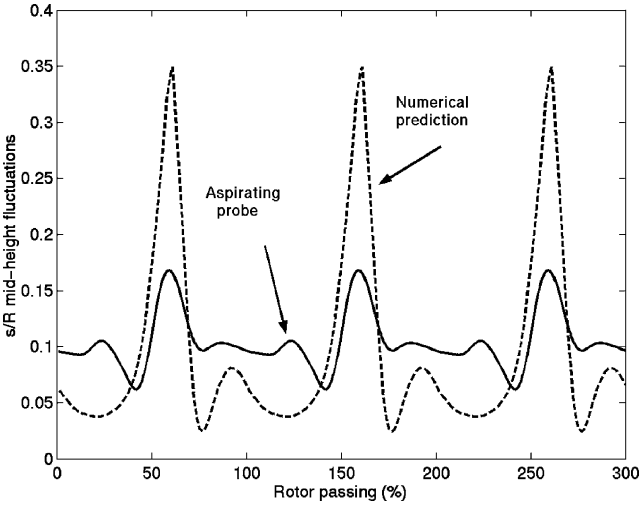

Fig. 6. Comparison of entropy/R at mid-height with numerical prediction.

total pressure and total temperature are measured simultaneously both spatially and temporally.

A direct comparison of the total pressure can be made with previous experimental measurements, since this has been measured using both a wedge and a pyramid probe in the same facility at the same operating conditions. These probes both use silicon piezoresistive pressure sensors to measure total pressure, Mach number and yaw angle, the pyramid probe also measuring pitch angle (Ainsworth et al., 2000). All three measurements were made at mid-height at one vane position on a plane approximately 15% of axial chord behind the rotor trailing edge. The three measurements show good overall agreement, Fig. 5, both in the mean levels and in the magnitude and position of the fluctuations and thus give a high degree of confidence in the measurement of entropy. The differences are mainly due to slight differences in the probe positions and the spatial averaging performed by the probes, each of which is a slightly different shape, although very similar in size.

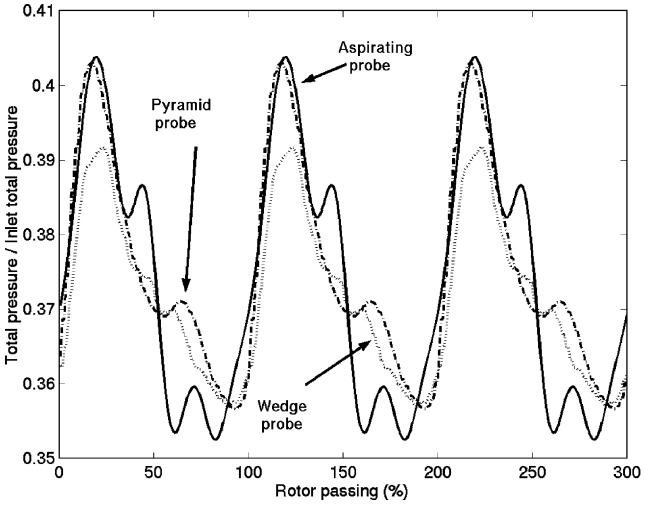

Fig. 5. Comparison of total pressure at 31% vane passing at mid-height relative to stage inlet.

The experimental measurements made at mid-height were then compared with the Unstrest predictions, shown in Fig. 6 for entropy/R. Although there is good general agreement, the numerical prediction over-predicts the entropy generated in the wake. However, since the numerical prediction is run without any heat transfer, the effect of this on the generation of entropy has to be checked. For reversible heat transfer, the entropy change at mid-height due to heat transfer can be calculated by integrating over the axial length of both rotor blades:

$$\Delta S = \int_{\mathrm{BS}} \frac{\mathrm{d}Q}{T}. \tag{7}$$

The heat transfer can be calculated using the blade surface heat transfer coefficient and the resulting increase in entropy, denoted s', is integrated over the complete rotor blade pitch:

$$\int_P s' \cdot \rho u \cdot r \,\mathrm{d}\theta = -\int_{\mathrm{BS}} \frac{h(T - T_{\mathrm{BS}})}{T} \,\mathrm{d}x_{\mathrm{BS}}. \tag{8}$$

To estimate the passage-averaged, mass-weighted increase in entropy due to heat transfer, the heat transfer integral is assumed to be approximately constant:

$$\frac{s'}{R} \approx \frac{\bar{h}}{\dot{m}R}\left(\frac{T_{\mathrm{BS}}}{\overline{T}} - 1\right) l_{\mathrm{BS}}, \tag{9}$$

where the mass flow is calculated per rotor passage and the blade surface length includes both surfaces, over which a mean temperature ratio and heat transfer coefficient are assumed.

Previous experimental measurements on the same blade row (Moss et al., 1997) give approximate values of area-averaged heat transfer coefficient of 2300 W/m^2 K,

and temperature ratio of 1.14, which, for a mass flow of 0.5 kg/s per passage, gives a passage-averaged drop in entropy/R of approximately 0.0044. However, since this is likely to be concentrated in the wake region, the local effect will be slightly larger. Since this is small in comparison with the entropy generated in the wake, approximately 0.05, Fig. 4, the entropy due to heat transfer can be safely neglected in comparison with the entropy due to loss here. Although the entropy generated due to heat transfer to the upstream vanes is approximately twice that due to the rotor heat transfer, due to the larger temperature difference, by rotor exit the entropy increase due to heat transfer will have been smoothed out much more over the blade passage. This will thus be small in comparison with the relatively large increase in passage-averaged entropy due to irreversibilities in the flow.

It has been shown that the main source of inaccuracy in two-dimensional loss predictions is errors in the boundary layer loss prediction. This is because there is little entropy generated due to shock loss, and errors in the mixing loss are likely to be small, since all mixing processes obey the fundamental conservation equations that also govern the behaviour of the numerical predictions. However, the experimental measurements were made very close to the rotor trailing edge, by which stage mixing is incomplete: the numerical prediction of the mixing loss at this plane is thus likely to be inaccurate, even though the fully mixed out loss might be more accurate. The wake shape and loss may thus not be very well predicted. The error in the boundary layer loss prediction is likely to be due to approximations in the turbulence modelling and in the modelling of the near end wall region. The possible experimental errors will be investigated in more detail once the three-dimensional loss structure has been examined and the efficiency estimated.

5. Three-dimensional rotor dependent flow structure

Again, before examining the aspirating probe measurements, it is valuable to look at previous experimental measurements. A schematic of the rotor exit flow field, proposed by Miller et al. (2003) but not shown here, from previous experimental measurements shows four major flow features: trailing edge shock wave, wake, tip leakage vortex and lower passage vortex. The formation of the predicted loss structure through the rotor blades is then shown by the numerical prediction, Fig. 7. The inlet boundary layer is rolled up into passage vortices on the end walls, the upper passage vortex being dragged round the tip leakage vortex, such that by rotor exit it is relatively weak and found directly below the tip leakage vortex. All the rotor loss features migrate towards the tip due to the radial pressure gradient, and the

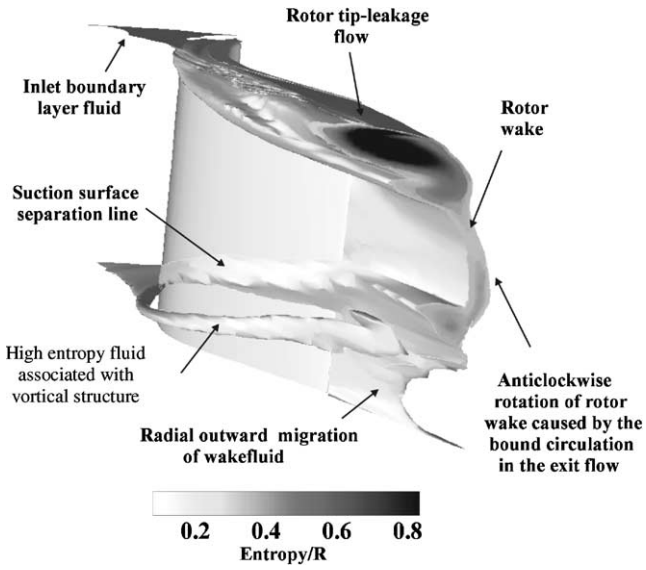

Fig. 7. Numerical prediction of formation of loss structure.

lower part of the wake is rolled up into the lower passage vortex, resulting in little wake fluid being found close to the hub end wall. There are thus expected to be four major loss features at exit: tip leakage vortex, upper passage vortex, wake and lower passage vortex. This is in excellent agreement with the experimental measurement of unsteady entropy, Fig. 8, where all of these features are clearly seen. The numerical prediction of rotor exit entropy is also shown, Fig. 9, for direct comparison. The experimental results were taken at 14 radial heights in the range 9.4–92.8% radial height.

The largest source of rotor loss is clearly the tip leakage vortex, which extends down to approximately 75% height and across nearly 75% of the blade pitch. The flow angle and Mach number variations in this region are also very large (Payne, 2001). The second largest source of rotor loss is the wake, which is strongest between approximately 30–70% radial height, leaning slightly to the left, looking upstream, due to the radial variation in blade exit whirl angle. It interacts at the tip with the tip leakage and upper passage vortices and at the hub with the lower passage vortex, which is found at approximately 30% height and 20% rotor pitch, in good agreement with the penetration height measured by Miller et al. (2003). Although all the rotor flow phenomena migrate radially outwards, the lower passage vortex migrates most rapidly since there is no end wall restriction.

Although the loss structure is predicted well, the entropy generation is over-predicted, particularly in the wake, which will affect its interaction with the lower passage vortex. The predicted wake extends down to the hub end wall more clearly than was seen experimentally, despite being weaker below the lower passage vortex. The thickness of the predicted end wall boundary layer,

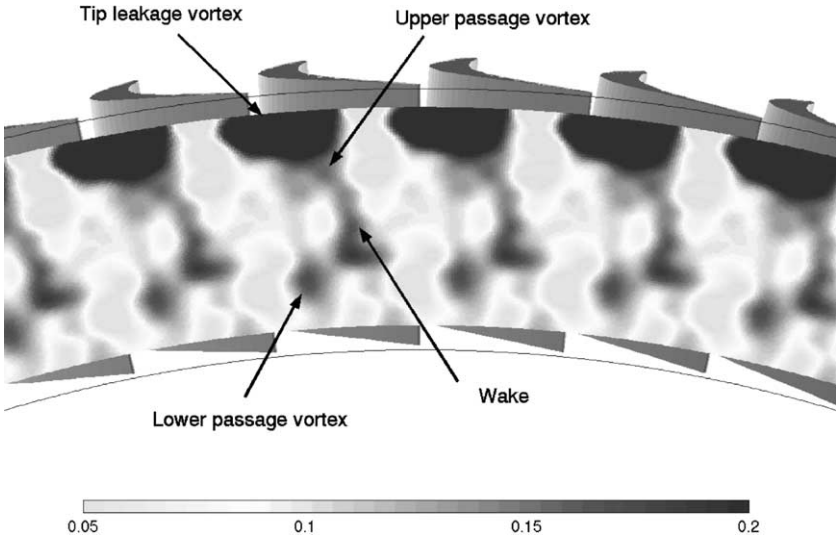

Fig. 8. Experimental entropy/R contour plot at 31% vane passing.

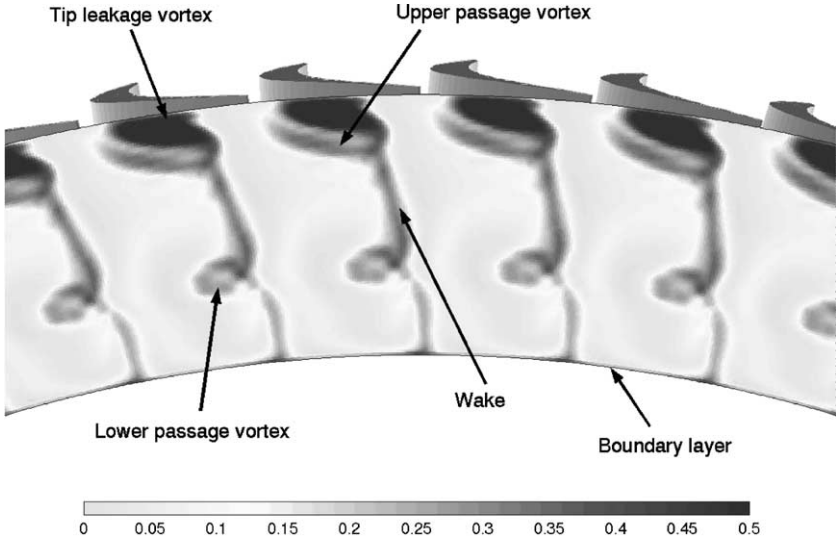

Fig. 9. Numerical prediction of entropy/R contour plot at 31% vane passing.

and hence the strength of the lower passage vortex, is largely dependent upon the assumption of a fully turbulent end wall. This remains to be validated and will also affect the loss mechanisms near the hub end wall. The only other source of loss is the hub end wall boundary layer, which is outside the experimental measurement range. However, this is a relatively small source of loss in comparison with the other secondary loss mechanisms.

6. Stage efficiency

Following on from a qualitative assessment of the loss structure, a quantitative assessment of the effects of the sources of loss on the stage efficiency can be made, which will also provide a quantitative estimate of the accuracy of the loss predictions. This is vital in improving blade design and in validating the use of numerical predictions to predict blade efficiency. The comparison of time-averaged entropy over radial height, Fig. 10, shows that the entropy level is extremely well predicted. It can be seen in Fig. 6 that, despite quite large differences in the structure over rotor phase, the mean level is in good agreement. The small peak in entropy at approximately 35% height is due to the interaction between the wake and the lower passage vortex, whereas the large peak at approximately 90% height is due to the tip leakage vortex. The radial position of the first peak is well predicted but the second is predicted to be slightly higher than was measured: this is probably due to slight differences in radial migration. The position

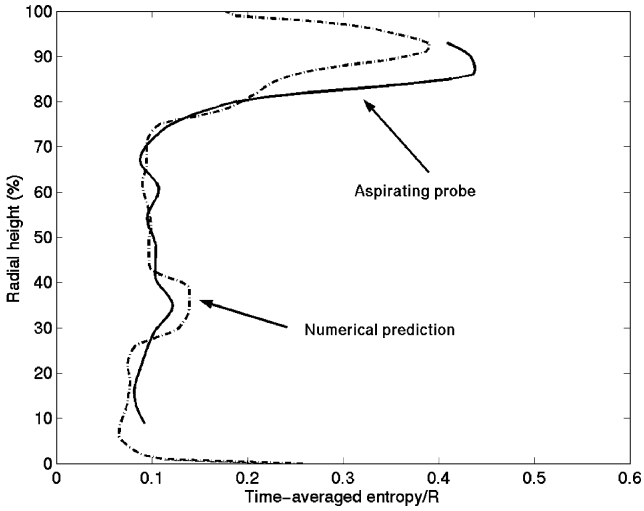

Fig. 10. Time-averaged entropy/R over radial height.

of the first peak agrees well with the measurement of the penetration height by Miller et al. (2003) of 38% experimentally and 39% numerically.

To quantify the different sources of loss, the flow field is divided into three regions: the primary flow, where the entropy is below a certain threshold value, the tip leakage flow and the remainder of the rotor loss flow field, comprising mainly the wake and lower passage vortex. Since the rotor loss mechanisms are associated with regions of low velocity fluid, the contributions of the entropy rise to the drop in efficiency must be mass-weighted:

$$\frac{\bar{s}}{R} = \frac{\int \left(\frac{s}{R}\right) \rho u \, \mathrm{d}A}{\int \rho u \, \mathrm{d}A}. \tag{10}$$

However, since there is no measurement of the mass flux, this is provided by the numerical calculations as a first approximation, since the agreement in the positions of the loss features is good. The entropy readings in the end wall regions are also provided by the numerical predictions. Once the mean primary flow entropy has been calculated, the entropy in the remaining flow regions above this value is area averaged over the blade passage. This procedure is then performed for both the measurements and the predictions, Table 2.

There is excellent agreement in the total entropy rise and good agreement in the breakdown of loss, which confirms the agreement seen in the secondary flow structure. The only slight difference is that the loss outside the tip leakage vortex is experimentally found to be comprised more of the primary flow loss than the remaining loss. This agrees with the results at mid-height, where there is predicted to be a sharper peak in entropy at the wake than was found experimentally. Only the total pressure ratio is then required to convert these entropy rises to efficiency drops, Eq. (1) and Table 3: this is taken to be the time–mean pressure ratio from the mid-height stationary probes. Although a mixing approach should strictly be used, a local definition of efficiency at this measurement plane gives a good estimate of the relative contributions of the different flow regions to the total efficiency drop.

Table 2
Mass-weighted, passage-averaged entropy/R rise due to different regions of the flow field

	Aspirating probe	Numerical calculation
Primary flow	0.0785	0.0592
Tip leakage flow	0.0344	0.0360
Remainder of loss	0.0136	0.0263
Total entropy/R rise	0.1265	0.1215

Table 3
Efficiency drops due to different regions of the flow field

	Aspirating probe	Numerical calculation
Primary flow	7.53%	5.66%
Tip leakage flow	3.28%	3.43%
Remainder of loss	1.30%	2.50%
Total loss	12.10%	11.59%
Stage efficiency	87.90%	88.41%

The drop in stage efficiency due to the tip gap can be compared with the measurements made by Harvey and Ramsden (2000), who found that the fully mixed out efficiency drops by 2.3% per 1% tip gap/span. For the tip gap of 2.25%, the expected efficiency drop is thus 5.2%. This is somewhat larger than was found both experimentally and numerically, as would be expected as the tip leakage loss will increase as the flow mixes out. In a multi-stage turbine, however, the flow is not fully mixed out before it reaches the next stage: thus our value provides a good estimate of the drop in efficiency prior to reaching the downstream stage. The correlation can also be used to compare the estimated stage efficiency of 87.9% with the stage efficiency as previously measured in a cold flow rig, which when adjusted to the same tip gap is 86.7%, Fig. 11. These are in very good agreement,

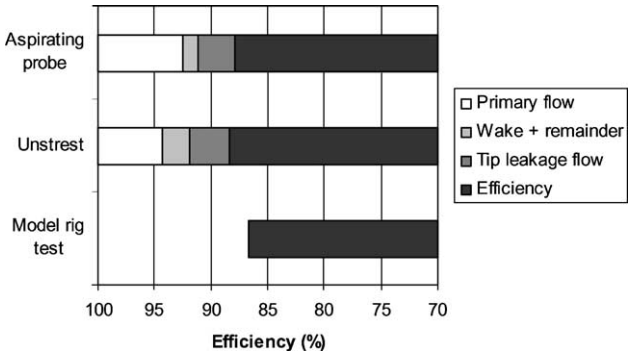

Fig. 11. Breakdown of efficiency.

with the numerical prediction also being very close. The small differences are probably partly due to the use of the numerically predicted mass flux and entropy in the near end wall regions. This very good agreement, together with the good agreement in total pressure at mid-height, indicates that the absolute accuracy of the experimental entropy is likely to be very high. Apart from the tip leakage vortex, the rotor loss causes only a small drop in efficiency, particularly with respect to the primary flow. It should also be noted that the measurements and numerical predictions have only considered the flow field at one vane position: more detailed experimental measurements over all vane positions are thus required to make a complete comparison with the measured stage efficiency.

7. Summary and conclusions

Unsteady experimental entropy measurements at one vane position at exit from a high pressure turbine stage at engine-representative conditions have enabled the rotor-dependent loss mechanisms and their effects on the stage efficiency to be quantified for the first time. These unique measurements have shown that there are four major loss mechanisms: the tip leakage vortex, the upper passage vortex, the wake and the lower passage vortex. The shock wave generates little entropy, since it is very weak, but large rises in both total pressure and total temperature. The tip leakage vortex causes an efficiency drop of 3.3%, less than that found from mixed out flow measurements, since the measured flow field is close to the rotor trailing edge. There is also an excellent agreement with the overall stage efficiency: 87.9% compared to the actual value of 86.7%. The secondary losses outside the tip leakage vortex are small, with the primary flow being the largest cause of loss, 7.5%. This is an important finding, as it implies that the vane loss has mixed out across the passage, and will be discussed in a future paper.

The numerical prediction provides both an excellent qualitative estimate of the flow field and a very good prediction of the efficiency, although the wake entropy is over-predicted. It could thus be used to provide a greater understanding of the development of the various sources of loss, particularly the primary loss, in the future. Entropy measurements over all vane positions will also be required to make a more detailed study of the flow field. The effects of blade row interaction on each of these sources of loss and the stage efficiency will thus be examined in a future paper.

Acknowledgements

The authors gratefully acknowledge the support of Kevin Grindrod as well as others from the Oxford Rotor Group. They also wish to acknowledge the support of Rolls-Royce plc, the UK Ministry of Defence, DTI CARAD and QinetiQ, and thank them for permission to publish this work. Stephen Payne was supported by an EPSRC studentship.

References

Ainsworth, R.W., Shultz, D.L., Davies, M.R.D., Forth, C.J.P., Hilditch, M.A., Oldfield, M.L.G., Sheard, A.G., 1988. A transient flow facility for the study of the thermofluid dynamics of a full stage turbine under engine representative conditions. ASME Paper No. 88-GT-144.

Ainsworth, R.W., Miller, R.J., Moss, R.W., Thorpe, S.J., 2000. Unsteady pressure measurement. Measurement Science & Technology 11, 1055–1076.

Alday, J., Osborne, D.J., Morris, B., Ng, W., Gertz, J., 1993. Flow randomness and tip losses in transonic rotors. ASME Paper No. 93-GT-189.

Bindon, J.P., 1988. The measurement and formation of tip clearance loss. ASME Paper No. 88-GT-203.

Brayton, S.N., 1996. Hot wire instrumentation for unsteady aerodynamic measurements in a rotating gas turbine stage. D.Phil. Thesis, University of Oxford.

Brouckaert, J.F., 1998. Experience with a double-hot-wire aspirating probe in a transonic turbine stage. In: Proceedings of the 14th Symposium on Measuring Techniques for Transonic and Supersonic Flows in Cascades in Turbomachines, Limerick.

Bruun, H.H., 1995. Hot-Wire Anemometry: Principles and Signal Analysis. Oxford University Press.

Buttsworth, D.R., Jones, T.V., Chana, K.S., 1997. Unsteady total temperature measurements downstream of a high pressure turbine. ASME Paper No. 97-GT-407.

Collis, D.C., Williams, M.J., 1959. Two-dimensional convection from heated wires at low Reynolds numbers. Journal of Fluid Mechanics 6, 357–389.

Denton, J.D., 1990. The calculation of three-dimensional viscous flow through multistage turbomachines. ASME Paper No. 90-GT-19.

Denton, J.D., 1993. Loss mechanisms in turbomachines. ASME Paper No. 93-GT-435.

Harvey, N.W., Ramsden, K., 2000. A computational study of a novel turbine rotor partial shroud. ASME Paper No. 2000-GT-668.

Hodson, H.P., 1984. Measurements of wake-generated unsteadiness in the rotor passages of axial-flow turbines. ASME Paper No. 84-GT-116.

Mee, D.J., Baines, N.C., Oldfield, M.L.G., 1990. An examination of the contributions to loss on a transonic turbine blade in cascade. ASME Paper No. 90-GT-264.

Miller, R.J., Moss, R.W., Ainsworth, R.W., Horwood, C.K., 2003. Time-resolved vane–rotor interaction in high pressure turbine stage. Journal of Turbomachinery 125, 1–13.

Moore, H., Gregory-Smith, D.G., 1996. Transition effects on secondary flows in a turbine cascade. ASME Paper No. 96-GT-100.

Moss, R.W., Ainsworth, R.W., Garside, T., 1997. Effects of rotation on blade surface heat transfer: an experimental investigation. ASME Paper No. 97-GT-188.

Ng, W.F., Epstein, A.H., 1983. High-frequency temperature and pressure probe for unsteady compressible flows. Review of Scientific Instruments 54, 1678–1683.

Ng, W.F., Epstein, A.H., 1984. Unsteady losses in transonic compressors. ASME Paper No. 84-GT-183.

Parantheon, P., Lecordier, J.C., Petit, C., 1983. Dynamic sensitivity of the constant-temperature hot-wire anemometer to temperature fluctuations. TSI Quarterly 9, 3–8.

Payne, S.J., 2001. Unsteady loss in a high pressure turbine stage. D.Phil. Thesis, University of Oxford.

Prato, J., Lakshminarayana, B., 1992. Investigation of compressor rotor wake structure at peak pressure rise coefficient and effects of loading. ASME Paper No. 92-GT-32.

Roberts, Q.D., Denton, J.D., 1996. Loss production in the wake of a simulated subsonic turbine blade. ASME Paper No. 96-GT-421.

Sharma, O.P., Butler, T.L., 1986. Predictions of endwall losses and secondary flows in axial flow turbine cascades. ASME Paper No. 86-GT-228.

Sheard, A.G., 1989. Aerodynamic and mechanical performance of a high pressure turbine stage in a transient wind tunnel. D.Phil. Thesis, University of Oxford.

Sieverding, C.H., 1984. Recent progress in the understanding of basic aspects of secondary flows in turbine blade passages. ASME Paper No. 84-GT-78.

Suryavamshi, N., Lakshminarayana, B., Prato, J., 1996. Aspirating probe measurements of the unsteady total temperature field downstream of an embedded stator in a multistage axial flow compressor. ASME Paper No. 96-GT-543.

Van Zante, D.E., Suder, K.L., Strazisar, A.J., Okiishi, T.H., 1994. An improved aspirating probe for total-temperature and total-pressure measurements in compressor flows. ASME Paper No. 94-GT-222.

Wallace, J.D., Davies, M.R.D., 1997. Entropy generation measurement in a laminar turbine blade boundary-layer. ASME Paper No. 97-GT-450.

Yamamoto, A., Kaba, K., Matsunuma, T., 1995. Measurement and visualisation of three-dimensional flows in a linear turbine cascade. ASME Paper No. 95-GT-341.

Yaras, M.I., Sjolander, S.A., 1991. Prediction of tip leakage losses in axial turbines. ASME Journal of Turbomachinery 114, 204–210.